

# Composition and origin of nodules from the $\approx 20$ ka Pomici di Base (PB)-Sarno eruption of Mt. Somma – Vesuvius, Italy

Research Article

Rita Klébesz<sup>1,2\*</sup>, Robert J. Bodnar<sup>1†</sup>, Benedetto De Vivo<sup>2‡</sup>, Kálmán Török<sup>3§</sup>,  
Annamaria Lima<sup>2¶</sup>, Paola Petrosino<sup>2</sup>

<sup>1</sup> Dept. of Geosciences, Virginia Polytechnic Institute and State University,  
4044 Derring Hall, Blacksburg, VA 24061, USA

<sup>2</sup> Dept. of Earth Sciences, University of Naples "Federico II",  
Via Mezzocannone 8, Naples 80134, Italy

<sup>3</sup> Eötvös Loránd Geophysical Institute of Hungary,  
Columbus u. 17.-23., Budapest 1145, Hungary

Received 7 November 2011; accepted 6 February 2012

**Abstract:** Nodules (coarse-grain "plutonic" rocks) were collected from the ca. 20 ka Pomici di Base (PB)-Sarno eruption of Mt. Somma-Vesuvius, Italy. The nodules are classified as monzonite-monzogabbro based on their modal composition. The nodules have porphyrogranular texture, and consist of An-rich plagioclase, K-feldspar, clinopyroxene (ferroan-diopside), mica (phlogopite-biotite)  $\pm$  olivine and amphibole. Aggregates of irregular intergrowths of mostly alkali feldspar and plagioclase, along with mica, Fe-Ti-oxides and clinopyroxene, in the nodules are interpreted as crystallized melt pockets.

Crystallized silicate melt inclusions (MI) are common in the nodules, especially in clinopyroxenes. Two types of MI have been identified. Type I consists of mica, Fe-Ti-oxides and/or dark green spinel, clinopyroxene, feldspar and a vapor bubble. Volatiles (CO<sub>2</sub>, H<sub>2</sub>O) could not be detected in the vapor bubbles by Raman spectroscopy. Type II inclusions are generally lighter in color and contain subhedral feldspar and/or glass and several opaque phases, most of which are confirmed to be oxide minerals by SEM analysis. Some of the opaque-appearing phases that are below the surface may be tiny vapor bubbles. The two types of MI have different chemical compositions. Type I MI are classified as phono-tephrite – tephri-phonolite – basaltic trachy-andesite, while Type II MI have basaltic composition. The petrography and MI geochemistry led us to conclude that the nodules represent samples of the crystal mush zone in the active plumbing system of Mt. Somma-Vesuvius that were entrained into the upwelling magma during the PB-Sarno eruption.

**Keywords:** Mt. Somma-Vesuvius • nodules • melt inclusions • crystal mush zone

© Versita sp. z o.o.

\*E-mail: krita@vt.edu

†E-mail: rjb@vt.edu

‡E-mail: bdevivo@unina.it

§E-mail: torokklm@elgi.hu

¶E-mail: antima@unina.it

E-mail: petrosin@unina.it

## 1. Introduction

Nodules are foreign materials (xenoliths) found in erupted volcanic rocks. The term nodule usually refers specifically to coarse-grained “plutonic” xenoliths (e.g. [1–3]). In the Mt. Somma-Vesuvius literature, the term “nodules” has been used to describe a wide variety of rock types and textures. Hermes & Cornell [4] divided Mt. Somma-Vesuvius nodules into four groups: (1) biotite-bearing pyroxenite, wehrlite, and dunitite “accumulative” rocks; (2) “skarns”, represented by metasomatized carbonates; (3) recrystallized carbonate hornfels and (4) shallow plutonic rocks (“sub-effusive rocks”). Previous workers have studied these nodules extensively, especially the skarn and cumulate nodules from the younger Mt. Somma-Vesuvius eruptions [4–12]. Minerals in these nodules contain several different types of inclusions, including silicate melt, hydrosaline melt, and S-rich or CO<sub>2</sub>-rich fluids. The nodules and their inclusions could provide tools for understanding magmatic processes associated with the Mt. Somma-Vesuvius system, including crystallization and mixing histories of magmas, as well as hydrothermal processes, including ore metal transport and deposition [10].

Nodules from the Pomici di Base (PB)-Sarno eruption at Mt. Somma-Vesuvius, which are the focus of this investigation, have not been previously studied to our knowledge. These nodules are found almost exclusively in the final products of the PB-Sarno eruption, which are comprised of lithic-rich fall deposits, surges and flows. In other eruptions of Mt. Somma-Vesuvius (e.g. Avellino and 79 AD eruptions), nodules are also found in the early ash and pumice airfall phase. Our goal in this study is to constrain the origin of the PB-Sarno nodules, and to determine what additional information they might provide concerning the underlying magmatic system prior to the PB-Sarno eruption. In this paper we present a detailed description of the nodules found in the final products of the PB-Sarno eruption, including their petrography and mineral chemistry and preliminary results of melt inclusion (MI) studies.

## 2. Geological setting

Mt. Somma-Vesuvius is located at the southern end of the Campanian Plain, near the city of Naples in southern Italy. The Mt. Somma-Vesuvius volcanic complex comprises the older, truncated edifice of Mt. Somma, and Vesuvius, which forms a cone that developed within the older caldera by predominantly effusive activity (Fig. 1). Eruptive activity associated with the volcanic complex started after the huge Campanian Ignimbrite eruption (39 ka [13]),

but other volcanic activity in the area which is not related to Mt. Somma-Vesuvius dates back to ca 400 ka [14, 15] (and references therein). According to Santacroce et al. [15] the PB eruption represents the first explosive event of the Somma volcano, dated at ca 22 ka. Other authors [16, 17] refer to this event as the Sarno eruption, and report that it follows an older explosive event, the Codola eruption. We use the term PB-Sarno eruption to recognize the fact that the two different names are commonly used in the literature to refer to the same eruptive event.

Eruptive activity at Mt. Somma-Vesuvius is cyclical, and three mega-cycles can be distinguished based on bulk rock compositional data [18] (and references therein). Within each mega-cycle the primary magma composition remains the same, but a new mega-cycle is characterized by a different composition [17]. The compositions of the eruptive products of the 3 mega-cycles change from slightly, to mildly, to highly silica-undersaturated [15, 18]. The products of the first mega-cycle are slightly silica-saturated (K-trachyte, K-latitude) evolving toward slightly silica-undersaturated [17, 18]. The products of the second mega-cycle are mildly silica-undersaturated (phonotephrites to phonolites; [15, 17, 19]). The third mega-cycle is characterized by strongly silica-undersaturated rocks with tephrite to tephriphonolite-foiidite composition [15, 19]. Each mega-cycle is made up of several shorter cycles, each starting with a plinian or sub-plinian eruption, followed by a strombolian-vulcanian “interplinian” stage. The first mega-cycle lasted from >25 ka to about 14 ka, the second from 8 ka to 2.7 ka. The third mega-cycle began after ≈800 years of repose with the 79 AD eruption that destroyed Pompeii. The last eruption at Mt. Somma-Vesuvius took place in 1944 and it is not clear if this represents the closing event of the third mega-cycle, or if it represents the beginning of a repose time within the shorter cycle that began in 1631. As noted by De Vivo et al. [18], the current repose time (68 years) is anomalous for the 1631–1944 interplinian cycle in which eruption cyclicity was between 7 and 30 years [18] (and references therein).

The PB-Sarno eruption occurred in three phases: (1) the opening phase consisting of ash and minor pumice fall, followed by: (2) a plinian phase comprising up to 6.5 m of compositionally zoned (trachyte to latite) fallout deposits with minor surge deposits; and (3) the closing phreatomagmatic phase characterized by lithic-rich fall, surge and flow deposits [20, 21]. According to Bertagnini et al. [20] this was the largest eruptive event in the history of Mt. Somma-Vesuvius on the basis of the thickness and areal distribution of the erupted material.

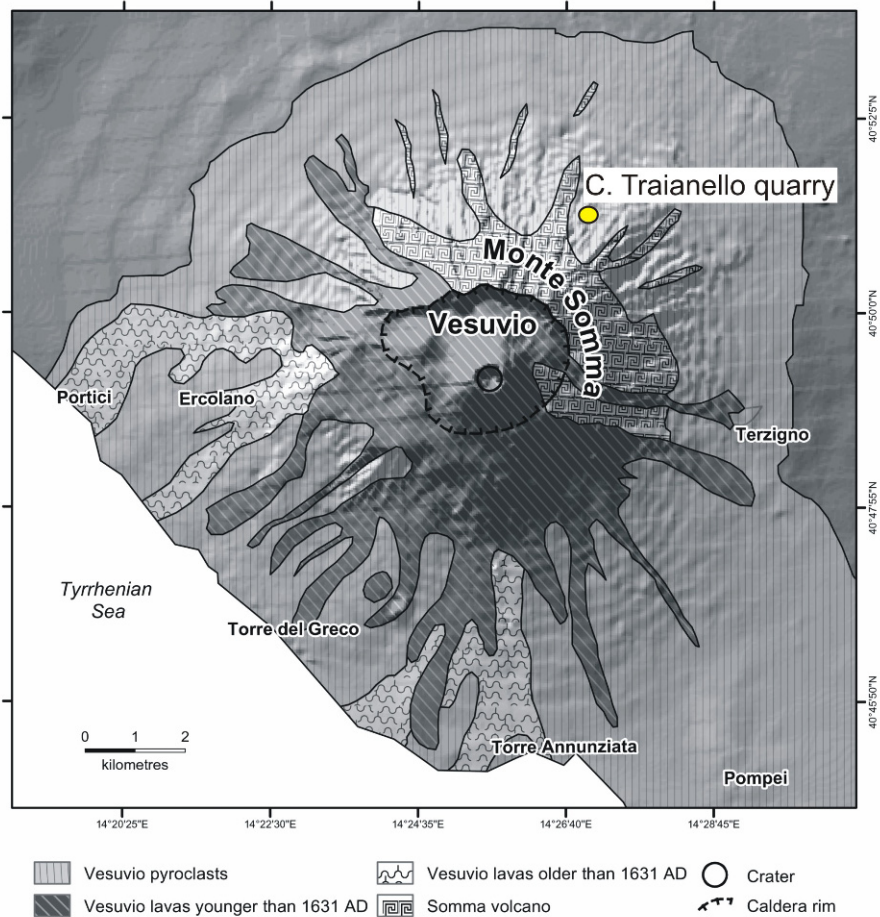


**Figure 1.** Map of Mt. Somma-Vesuvius – adapted from Peccerillo [40] – and the sample location within the C. Traianello quarry.

### 3. Samples and analytical methods

Samples were collected from the C. Traianello quarry, located on the NE slope of Mt. Somma (Fig. 1). All samples were collected from the topmost unit (about 1.5 m thick at the sample location) that consists of a pyroclastic flow deposit (Fig. 2). The studied nodules are coarse-grained (grain size up to 7 mm) igneous rocks with rounded to slightly angular equant to elongated shape. Nodule size varies from 1 to 5 cm. Nodules were divided into two sub-equal portions, and one portion was gently crushed by hand and clinopyroxene phenocrysts were handpicked under a binocular microscope. Single clinopyroxene crystals were polished on both sides, following procedures described by Thomas and Bodnar [22]. The other part of the nodule was used to prepare a doubly-polished thin section for analysis of phenocrysts by Cameca SX50 electron microprobe (EMPA) at Virginia Tech (Blacksburg, VA, USA).

A beam current of 20 nA and an accelerating voltage of 15 kV were used during the analyses for olivine, clinopyroxene, amphibole and mica. A 5  $\mu\text{m}$  defocused beam was used for feldspars, with analytical conditions similar to those described above for other minerals. The one sigma relative error is always less than 5%, and is usually under 1%, if the concentration of the element is >1 wt%.

Individual crystallized MI in single crystals extracted from the nodules during crushing were analyzed using an Excimer laser-ablation inductively-coupled plasma mass spectrometry (LA-ICPMS) system at Virginia Tech following the method described in Halter et al. [23]. Details of run conditions are reported in Table 1. The pit size was selected to be slightly larger than the inclusion diameter for each inclusion. The chemical composition of MI is quantified following the procedure described in Halter et al. [23], using the software package AMS [24]. The uncertainties are estimated to be 2–4% relative [25]. For

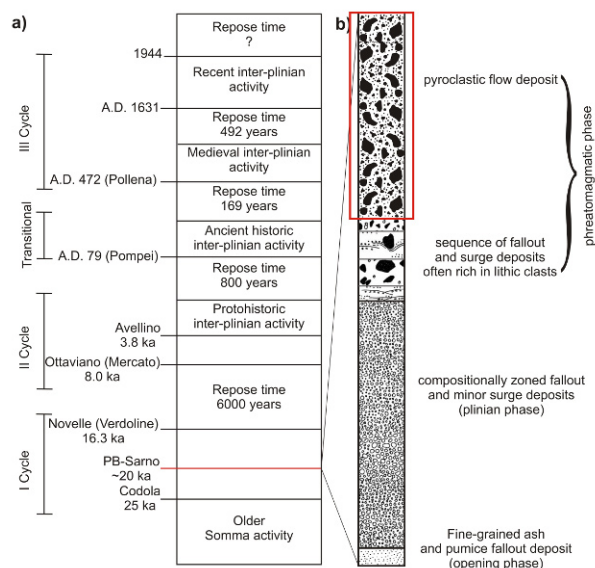


**Figure 2.** a) Stratigraphy of volcanic activity of Mt. Somma-Vesuvius, modified from Piochi et al. [25]. b) Schematic stratigraphic column of the PB-Sarno eruptive products, adapted from Bertagnini et al. [20]. The rectangular box near the top of the expanded column on the right indicates the portion of the unit that contains the nodules.

the internal standard, a value of  $\text{Al}_2\text{O}_3=18$  wt% was used, because the aluminum content of the magma varies little (15.2 to 19.8 wt%) during the early history (megacycle I and earlier) of Mt. Somma [17, 19, 21].

## 4. Petrography

In this study we have recognized two types of nodules (Type A and B) based on their modal composition. All of the samples display a porphyrogranular texture (larger crystals in a finer-grained polycrystalline matrix) and are compositionally classified as monzonite-monzogabbro.

Type A nodules contain euhedral clinopyroxene and euhedral to subhedral olivine phenocrysts (Fig. 3a-b). The clinopyroxene phenocrysts show minor compositional zoning, and they contain olivine, apatite and Fe-Ti-oxide mineral inclusions, as well as MI. The rims of the crystals are irregular and show abundant embayments (“jagged” rims), suggesting that locally the clinopyroxenes were out of equilibrium with the melt. Mica  $\pm$  clinopyroxene overgrowths are often observed around the olivine phenocrysts. The groundmass is completely crystallized, and consists of euhedral to subhedral (tabular) feldspar, clinopyroxene, mica, F-apatite and Fe-Ti-oxides. We also observed crystal aggregates comprised of irregular intergrowths of alkali feldspar and plagioclase, with lesser mica, Fe-Ti-

**Table 1.** LA-ICPMS instrument and data acquisition parameters.

Excimer 193-nm ArF laser GeoLasPro	
Output Energy	150 mJ
Energy Density on sample	$\sim 7 - 10$ J/cm <sup>2</sup>
Repetition Rate	5 Hz
Pit Size	Between 16 and 60 mm
Ablation Cell Volume	$\sim 1.5$ cm <sup>3</sup>
Cell Gas Flow (He)	$\sim 1$ L/min
Agilent 7500ce quadrupole ICP-MS	
Auxiliary gas flow	1.03 l/min Ar
RF power	1500 V
Detector Mode	Dual 8 orders of magnitude linear dynamic range
Quadrupole Settling Time 2 ms	
Data acquisition parameters	
Sweeps per reading	1
Reading per replicate	200 – 300
Replicates	1
Dwell time per isotope	10 ms
Points per peak	1 per measurement
External Standard	NIST610 glass
Isotopes Analyzed	<sup>23</sup> Na, <sup>25</sup> Mg, <sup>27</sup> Al, <sup>28</sup> Si, <sup>39</sup> K, <sup>40</sup> Ca, <sup>45</sup> Sc, <sup>49</sup> Ti, <sup>51</sup> V, <sup>52</sup> Cr, <sup>55</sup> Mn, <sup>56</sup> Fe, <sup>62</sup> Ni, <sup>85</sup> Rb, <sup>88</sup> Sr, <sup>89</sup> Y, <sup>90</sup> Zr, <sup>93</sup> Nb, <sup>138</sup> Ba, <sup>139</sup> La, <sup>140</sup> Ce, <sup>143</sup> Nd, <sup>147</sup> Sm, <sup>153</sup> Eu, <sup>172</sup> Yb

oxides and clinopyroxene (Fig. 3c). The size of the aggregates ranges from about 100  $\mu\text{m}$  up to a few mm. Crystals in the aggregates are much smaller than those in the groundmass. Based on the petrographic characteristics described above, we interpreted the aggregates to represent crystallized melt pockets.

The dominant phenocryst in Type B nodules is sub- to anhedral amphibole (Fig. 3d-e). A reaction rim, consisting of mica, clinopyroxene and feldspar, is sometimes observed around the amphiboles. The edges of the amphibole phenocrysts are more irregular compared to the clinopyroxene phenocrysts in type A nodules. The groundmass consists of clinopyroxene, K-feldspar, Fe-Ti oxide, F-apatite and an unidentified Ca-K-silicate phase. Crystal aggregates are also observed and consist of irregular intergrowths of K-feldspar and the same unidentified Ca-K-phase as in the groundmass, with abundant mica and Fe-Ti-oxides. The crystal aggregates range up to a few hundred microns. The aggregates and the groundmass show similar textures, except that the aggregates are finer grained. Based on the petrographic characteristics we interpret the aggregates to represent crystallized melt pockets, similar to those in Type A nodules.

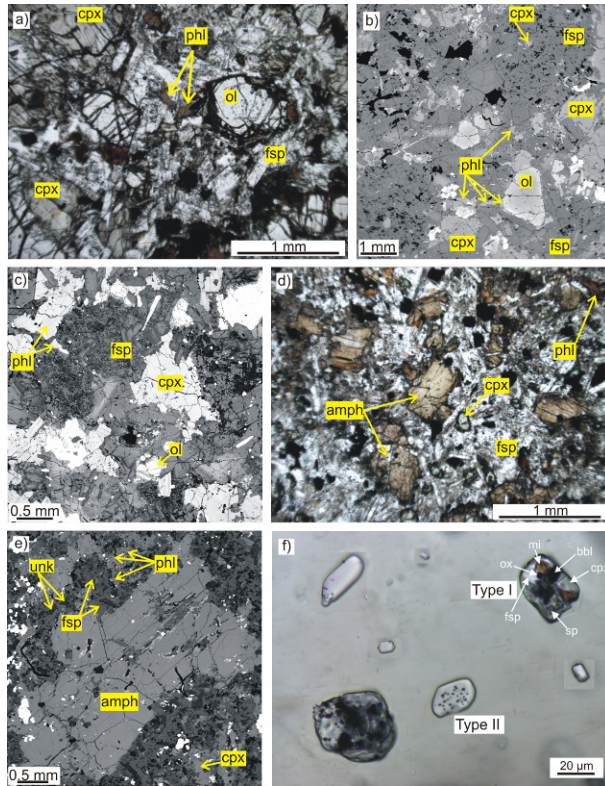


**Figure 3.** Photomicrographs showing mineral textures and melt inclusions in the nodules. a) Photomicrograph (in plane polarized light) of Type A nodule showing a porphyrogranular texture with clinopyroxene (cpx) and olivine (ol) phenocrysts. The matrix consists of feldspar (fsp), phlogopite (phl), apatite and Fe-Ti-oxides. b) Scanning electron microscope back-scattered (BSE) image of Type A nodule. Aggregates of cpx, phl and irregular intergrowths of alkali feldspar and plagioclase can be observed. c) BSE image of Type A nodule at higher contrast and higher magnification compared to image "b". The irregular intergrowth of feldspars in the groundmass is highlighted (lighter areas are alkali feldspar, and darker areas are plagioclase). d) Photomicrograph (in plane polarized light) of Type B nodule showing a porphyrogranular texture with amphibole (amph) phenocrysts. The matrix consists of cpx, phl, fsp, apatite and Fe-Ti-oxides. e) BSE image of Type B nodules. Note the irregular intergrowth of phl, fsp and an unknown phase (unk) adjacent to the amph phenocryst. f) Photomicrograph of Type I and Type II melt inclusions in cpx from Type A nodule. Type I consists of mica (mi), Fe-Ti-oxides (ox) and/or dark green spinel (sp), clinopyroxene (cpx), feldspar (fsp) and a vapor bubble (bb). Type II Inclusions are generally lighter in color and they contain feldspar and/or glass and several dark phases that are possibly oxide minerals and/or tiny vapor bubbles.

## 5. Mineral chemistry

Compositions of representative mineral phases in the nodules are listed in Table 2. Clinopyroxene is present as phenocrysts and in the groundmass in Type A nodules, while it only appears in the groundmass in Type B nodules. Clinopyroxenes have diopside-ferroan diopside com-

positions ( $\text{En}_{49-33}\text{Wo}_{46-47}\text{Fs}_{5-20}$ ) in Type A nodules, and a ferroan diopside composition ( $\text{En}_{39-24}\text{Wo}_{48-49}\text{Fs}_{13-27}$ ) in Type B nodules (Fig. 4a). The mg# ( $\text{Mg}/(\text{Mg}+\text{Fe}^{\text{tot}})$ ) ranges from 0.92 to 0.63 in Type A nodules, and from 0.79 to 0.49 in Type B nodules. The clinopyroxenes generally show normal zoning, but rarely show reverse zoning. The composition of the clinopyroxene in the groundmass is similar to the composition of the rims of clinopyroxene phenocrysts, suggesting that the groundmass clinopyroxenes crystallized as a result of rapid cooling of the same melt that was crystallizing at the rims of clinopyroxene phenocrysts.

Olivine phenocrysts were only observed in Type A nodules. The Fo content of olivine ( $\text{Mg}^*/100/(\text{Mg}+\text{Fe})$ ) ranges from 76 to 54. The olivines have uniformly low NiO (<0.16 wt%) and relatively high CaO content (up to 0.36 wt%).

Micas in both nodule types are fluorine-rich phlogopites, but the composition in Type A nodules has a wider range (Fig. 4b). The mg# ( $\text{Mg}/(\text{Mg}+\text{Fe}^{\text{tot}})$ ) ranges from 0.88 to 0.59 and from 0.90 to 0.86, in Type A and B nodules, respectively. The F content ranges from 6.5 wt% to 2.3 wt% in Type A, and from 8.3 wt% to 7.2 wt% in Type B nodules.

Feldspar is the main component of the groundmass. K-feldspar and plagioclase are equally abundant in type A nodules, but K-feldspar is much more abundant than plagioclase in type B nodules. Intergrowth feldspars in Type A nodules are enriched in K and Na compared to the tabular feldspars in the same nodule (Fig. 4c). Many tabular K-feldspars have a Ba-rich core (up to 6 wt%), with Ba content decreasing gradually towards the rim to, in some cases, below detection limit.

Magnesio-hastingsite amphiboles with small variations in FeO (7.3-9.7 wt%), MgO (15.6-17.4 wt%) and F content (3.6-4.8 wt%) occur as phenocrysts in Type B nodules. Accessory apatite in both types of nodules is extremely F-rich (up to 6 wt%).

Landi et al. [21] described both polycrystalline and plagioclase-only aggregates in the pumice and scoria that were deposited during the plinian phase of the PB-Sarno eruption. They interpreted the aggregates to represent fragments of the crystal mush zone at the upper margins of the magma chamber that were entrained into the erupting material. The compositions of plagioclase and sanidine in the aggregates described by Landi et al. [21] are similar to those in our samples (Fig. 4c). They also report clinopyroxene, but with a more evolved composition ( $\text{Fs}_{20-24}$ ) compared to that found in this study, and potassium-ferripargasite amphibole, which is also different from the magnesio-hastingsite amphibole in our samples.

**Table 2.** Representative microprobe analyses of the mineral phases in Type A and B nodules from the Sarno eruption (gm - groundmass, agg. - irregular intergrowth of feldspar in the aggregates, mg#=Mg/(Mg+Fe), b.d. -below detection).

Clinopyroxene																																			
Sample	Type A					Type B																													
	core	rim	zone	core	rim	gm	gm	gm	gm	rim																									
SiO <sub>2</sub>	54.60	51.16	51.46	51.98	51.26	50.69	49.10	50.64	50.91	43.10	43.29	42.90	SiO <sub>2</sub>	38.20	39.90	40.92																			
TiO <sub>2</sub>	0.22	1.01	0.98	0.82	1.16	1.50	1.43	0.73	0.67	0.85	1.21	1.08	TiO <sub>2</sub>	4.88	6.80	1.94																			
Al <sub>2</sub> O <sub>3</sub>	1.93	4.09	4.06	4.00	3.29	3.73	6.50	4.60	3.33	11.77	11.85	11.75	Al <sub>2</sub> O <sub>3</sub>	13.72	12.97	13.33																			
FeO	2.88	7.99	7.52	6.54	8.57	9.18	7.76	8.07	10.64	8.64	7.31	9.71	FeO	16.43	8.39	5.71																			
MnO	0.05	0.16	0.16	0.13	0.13	0.17	0.23	0.21	0.45	0.15	0.16	0.31	MnO	0.16	0.07	0.22																			
MgO	17.88	14.28	14.48	14.77	13.84	13.13	13.25	13.02	11.27	16.95	17.15	15.57	MgO	13.50	18.26	22.75																			
CaO	22.95	22.02	22.02	22.83	22.32	22.34	22.42	23.05	22.75	12.71	12.84	12.33	CaO	0.03	0.16	0.01																			
Na <sub>2</sub> O	0.19	0.36	0.36	0.27	0.34	0.38	0.34	0.38	0.49	1.92	1.81	0.93	Na <sub>2</sub> O	0.65	0.54	0.11																			
Total	100.69	101.06	101.03	101.34	100.91	101.12	101.02	100.70	100.51	2.06	2.50	4.02	K <sub>2</sub> O	9.45	9.53	9.94																			
En	50	41	42	42	40	38	39	38	33	4.64	4.43	3.59	F	3.00	4.25	7.70																			
Wo	46	46	46	47	46	47	48	48	48	0.10	0.10	0.10	Cl	0.11	0.07	0.04																			
Fs	5	13	12	11	14	15	13	14	18	102.89	102.64	102.28	total	100.14	100.95	102.67																			
Feldspar										Olivine					Apatite					Unknown phase															
Sample	Type A			Type B			Sample	Type A			Sample	Type A			Sample	Type B			Sample	Type B															
	core	rim	agg.	core	rim	agg.		SiO <sub>2</sub>	FeO	MnO		NiO	MgO	CaO		Total	SiO <sub>2</sub>	FeO		MnO	CaO	Total	SiO <sub>2</sub>	TiO <sub>2</sub>	Al <sub>2</sub> O <sub>3</sub>	Cr <sub>2</sub> O <sub>3</sub>	MgO	CaO	MnO	FeO	Na <sub>2</sub> O	K <sub>2</sub> O	F	Cl	Total
SiO <sub>2</sub>	62.10	65.55	64.95	48.42	63.51	61.79	65.17	SiO <sub>2</sub>	38.27	35.24	P <sub>2</sub> O <sub>5</sub>	38.79	39.67	SiO <sub>2</sub>	37.39	37.55																			
Al <sub>2</sub> O <sub>3</sub>	19.90	19.13	19.83	32.35	23.12	22.81	19.38	FeO	24.23	33.44	SiO <sub>2</sub>	0.33	1.03	TiO <sub>2</sub>	b.d.	b.d.																			
CaO	0.90	0.75	1.06	16.69	5.05	0.61	0.78	MnO	0.34	0.87	CaO	54.70	54.03	Al <sub>2</sub> O <sub>3</sub>	28.96	29.68																			
Na <sub>2</sub> O	3.45	3.56	4.10	2.00	8.17	0.42	0.38	NiO	0.03	b.d.	FeO	0.43	0.28	Cr <sub>2</sub> O <sub>3</sub>	b.d.	b.d.																			
K <sub>2</sub> O	9.83	11.09	10.31	0.09	0.52	15.60	15.99	MgO	37.14	29.82	F	6.48	6.23	MgO	b.d.	b.d.																			
BaO	3.73	0.14	0.03	0.05	0.04	0.03	0.18	CaO	0.35	0.26	Cl	0.32	0.08	CaO	13.58	14.62																			
Total	99.90	100.22	100.29	99.60	100.40	101.25	101.87	Total	100.36	99.64	Total	101.05	101.32	Total	0.02	0.04																			
Ab	33	32	36	13	72	4	3	Fo	73	61				FeO	b.d.	b.d.																			
An	5	4	5	87	25	3	4							Na <sub>2</sub> O	0.97	1.33																			
Or	62	65	59	0	3	93	93							K <sub>2</sub> O	4.20	4.61																			
										mg#					0.59					0.80					0.88										

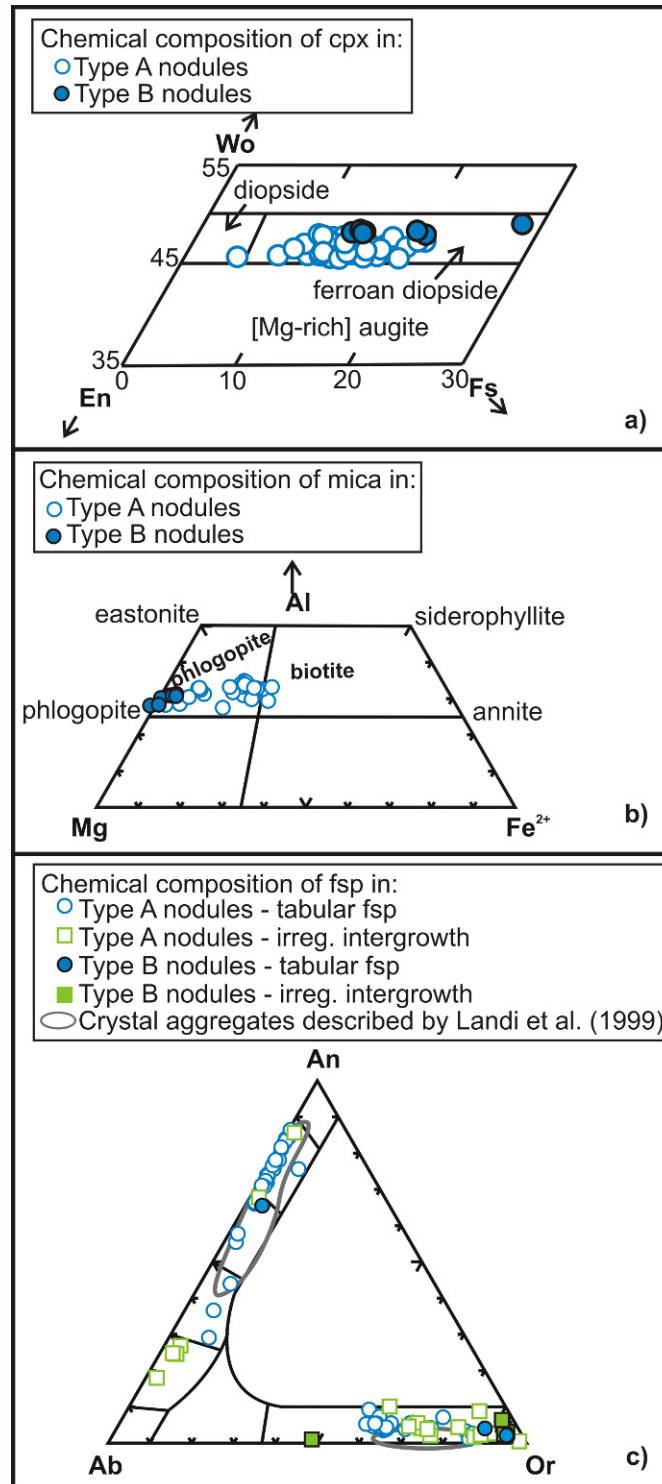


**Figure 4.** Chemical composition of minerals in Type A and B nodules: a) clinopyroxene (cpx), b) mica, and c) feldspar (fsp) compositions. For comparison, compositions of feldspars in crystal aggregates reported by Landi et al. [21] have been plotted.

**Table 3.** Representative LA-ICP-MS analysis of crystallized silicate-melt inclusions in clinopyroxene host from Type A nodule.

Sample	Type I					Trans.	Type II				
(wt%)											
SiO <sub>2</sub>	52.35	48.89	52.97	56.01	52.09	49.44	48.53	52.34	45.03		
TiO <sub>2</sub>	1.19	1.75	1.31	1.18	1.63	1.00	0.90	0.40	0.63		
Al <sub>2</sub> O <sub>3</sub>	17.83	18.01	18.01	18.01	18.00	17.92	18.00	18.01	18.00		
FeO	6.81	8.03	6.30	5.75	6.71	6.09	2.48	2.82	2.16		
MnO	0.14	0.12	0.13	0.08	0.11	0.11	0.11	0.08	0.11		
MgO	4.78	4.58	4.00	3.28	4.18	7.24	8.23	7.79	9.84		
CaO	7.60	8.11	7.26	4.12	8.30	13.21	19.55	16.19	21.89		
Na <sub>2</sub> O	2.73	1.24	3.09	3.08	2.52	1.37	1.40	1.04	1.31		
K <sub>2</sub> O	6.18	8.56	6.54	7.85	5.86	3.24	0.58	0.75	0.68		
Total	99.61	99.29	99.61	99.36	99.40	99.62	99.78	99.42	99.65		
(ppm)											
Ni	50	59	52	51	64	65	84	136	21		
Cr	< 0.156	267	<0.108	768	447	146	<0.314	2265	616		
V	251	206	242	106	294	320	253	201	183		
Sc	35	32	23	27	50	54	66	75	89		
Rb	215	272	239	306	201	111	4	17	10		
Ba	2237	3541	2350	2847	2589	1294	562	476	552		
Nb	33	48	41	45	42	14	1	3	1		
Sr	682	918	604	658	591	771	1008	979	1051		
Zr	202	261	244	207	247	113	59	55	49		
Y	26	33	27	15	29	20	17	11	14		
La	51	76	57	50	56	29	9	8	9		
Ce	100	152	117	89	110	62	29	25	24		
Nd	46	66	52	36	53	35	17	17	16		
Sm	8.8	15.3	9.8	7.2	12.7	4.1	1.5	3.1	7.4		
Eu	2.5	2.7	2.4	1.3	2.4	2.6	2.3	0.7	1.4		
Yb	2.5	2.3	2.7	<0.06	3.2	1.7	1.6	0.5	2.1		
MF	0.29	0.20	0.37	0.24	0.31	0.36	0.27	0.23	0.21		
host position	com-	En <sub>43</sub> Wo <sub>46</sub> En <sub>41</sub> Wo <sub>45</sub> En <sub>42</sub> Wo <sub>45</sub> En <sub>41</sub> Wo <sub>45</sub> En <sub>43</sub> Wo <sub>45</sub> En <sub>43</sub> Wo <sub>45</sub> En <sub>41</sub> Wo <sub>44</sub> En <sub>42</sub> Wo <sub>45</sub> En <sub>43</sub> Wo <sub>44</sub>									
MF - mass factor (mass of inclusion/total mass ablated); Trans. - Transitional type MI											

## 6. Melt inclusions

MI are abundant in clinopyroxenes in Type A nodules. All MI examined are partially to completely crystallized, which is typical of MI that cooled relatively slowly after trapping [26, 27]. The MI are mostly 20–30 μm in maximum dimension, but range from about 5 to 60 μm, and have rounded to angular shape.

MI are grouped into two types based on petrography (Fig. 3f). Type I consists of mica, Fe-Ti-oxide minerals and/or dark green spinel, clinopyroxene, feldspar and a vapor bubble. No volatiles (CO<sub>2</sub>, H<sub>2</sub>O) were detected in the bubbles by Raman spectroscopy [28]. Type II inclusions are generally lighter in color when observed in transmitted light and contain subhedral feldspar and/or

glass and several black (opaque?) phases, most of which are confirmed to be oxides by SEM analysis. Some of the opaque-appearing phases that are below the surface may be tiny vapor bubbles. The MI are either randomly distributed in the crystals or occur along a growth zone and are, therefore, interpreted to be primary. The two types of MI are spatially associated, appearing in the same area within the crystals. Type I MI comprises 70 to 80% of total melt inclusions observed. Moreover, some MI appear to be transitional between Types I and II in both their petrographic features and compositions. Only MI in clinopyroxenes from Type A nodules were analyzed.

Abundant data are available in the literature for comparison with our MI data. These include:

1. bulk rock compositions of pumices erupted during the plinian phase of the PB-Sarno eruption [17, 21]
2. bulk compositions of lavas erupted between 35–25 ka [17, 19]
3. bulk rock compositions of lava and scoria erupted after 25 ka but before the PB-Sarno eruption [19]
4. compositions of MI in clinopyroxene from lavas erupted between 35–25 ka, as well as compositions of MI from lavas that are younger than 25 ka but older than the PB-Sarno eruption [29]

The various types of data listed above have been plotted along with our MI data on various chemical discrimination diagrams, including total alkali-SiO<sub>2</sub> classification diagram (Fig. 5a; [30]), primitive mantle normalized [31] trace element diagrams (Fig. 5b–d), and major element variation diagrams (Fig. 5e–g). Because the Codola eruption ( $\sim 25$  ka) cannot be related to a specific Campanian source (i.e., Mt. Somma-Vesuvius, Campi Flegrei, or elsewhere in the Campanian region) [15, 16], it is not included in the comparison on Figure 5.

Our results indicate that Type I MI can be classified as phono-tephrite – tephri-phonolite – basaltic trachyandesite (Fig. 5a), and are similar to compositions of other MI from related eruptions [29]. The compositions of Type I MI from this study overlap with the compositions of the older Somma lavas (<35 ka but older than the PB-Sarno eruption) and show trends on major element variation diagrams that are similar to trends for MI from the literature [29] (Fig. 5e–g). The PB-Sarno pumices have a more evolved composition compared to the MI compositions of this study. However, trace element patterns for the Type I MI are similar to the older Somma lavas and the PB-Sarno pumices when plotted on primitive mantle normalized [31] trace element diagrams (Fig. 5b–d). Furthermore, the MI show enrichment in LILE (Rb, Ba, Th, K) and, to a lesser extent, HFSE (Nb, Zr) with respect to the primitive mantle.

Type II MI are mainly basaltic in composition, and show more primitive compositions with lower silica, alkalis and higher Ca and Mg content compared to published MI and bulk rock compositions (Fig. 5a, e–f). Type II MI show less enrichment in LILE and HFSE with respect to the primitive mantle, compared to Type I MI (Fig. 5b). Some MI could be classified as either type I or type II, based on petrography alone. These transitional MI appear to also show intermediate compositions (squares in Fig. 5).

Equilibrium between the MI and host was tested based on the Fe–Mg exchange reaction between clinopyroxene and host. Using the models in Putirka [32] that are based

on the Fe and Mg content of the melt and crystal, equilibration temperatures range from 1058 to 1264°C and pressures ranging from 3.9 to 10.6 kbar. Entering these temperatures into equation (35) of Putirka [32] predicts  $K_D(\text{Fe-Mg})^{\text{cpx-liq}}$  ranging from 0.25–0.29 over this range of temperatures, assuming that the melt and crystal are in equilibrium. However, the  $K_D(\text{Fe-Mg})^{\text{cpx-liq}}$  predicted from [32] for Type I MI ranges mostly from 0.3 to 0.45 (with a few values up to 0.6). This suggests that Type I MI were not in complete equilibrium with the host. The  $K_D(\text{Fe-Mg})^{\text{cpx-liq}}$  predicted for Type II MI are all  $>1$ , indicating that these MI compositions are far from equilibrium with the host.

Trends in MgO vs. CaO/Al<sub>2</sub>O<sub>3</sub> (Fig. 5h) for MI in this study are similar to trends defined by previously published MI data [29], and are consistent with melt compositions that would be produced during clinopyroxene fractionation from a crystallizing melt.

## 7. Discussion

The studied nodules were collected from the upper part of the PB-Sarno eruption deposits. As such, the nodules could have formed earlier from the same magma that produced the PB-Sarno eruption. Alternatively, the nodules might represent samples of older Somma volcanic activity (39–22 ka) that were ripped from the conduit walls and entrained into the PB-Sarno magmas as they ascended. Cioni et al. [33] found clear evidence of a caldera collapse associated with the PB-Sarno eruption, and Rolandi et al. [34] suggested that the PB-Sarno eruption was one of four eruptive events that contributed to the destruction of the older Somma cone. Therefore, it is likely that materials from the conduit walls and from older eruptive units have collapsed into the erupting PB-Sarno magma and were carried to the surface during the eruption.

Similarities between Type A and B nodules, including the presence of melt pockets, jagged (irregular) edges and slight zoning of the phenocrysts and the absence of typical equilibrium textures (e.g. planar boundaries, 120° jointing, absence of zoning) indicate that the two different nodule types formed in similar environments and experienced similar pre-eruptive histories. The textural features described above are common in the “sub-effusive” type of nodule described by Hermes & Cornell [4]. They interpret these nodules to have formed at a shallower level compared to the “accumulative” nodule type. These workers state additionally that the compositions of sub-effusive nodules and compositions of extruded lavas are similar. They suggest that the “sub-effusive” type of nodule represents samples of the crystal mush zone in which the

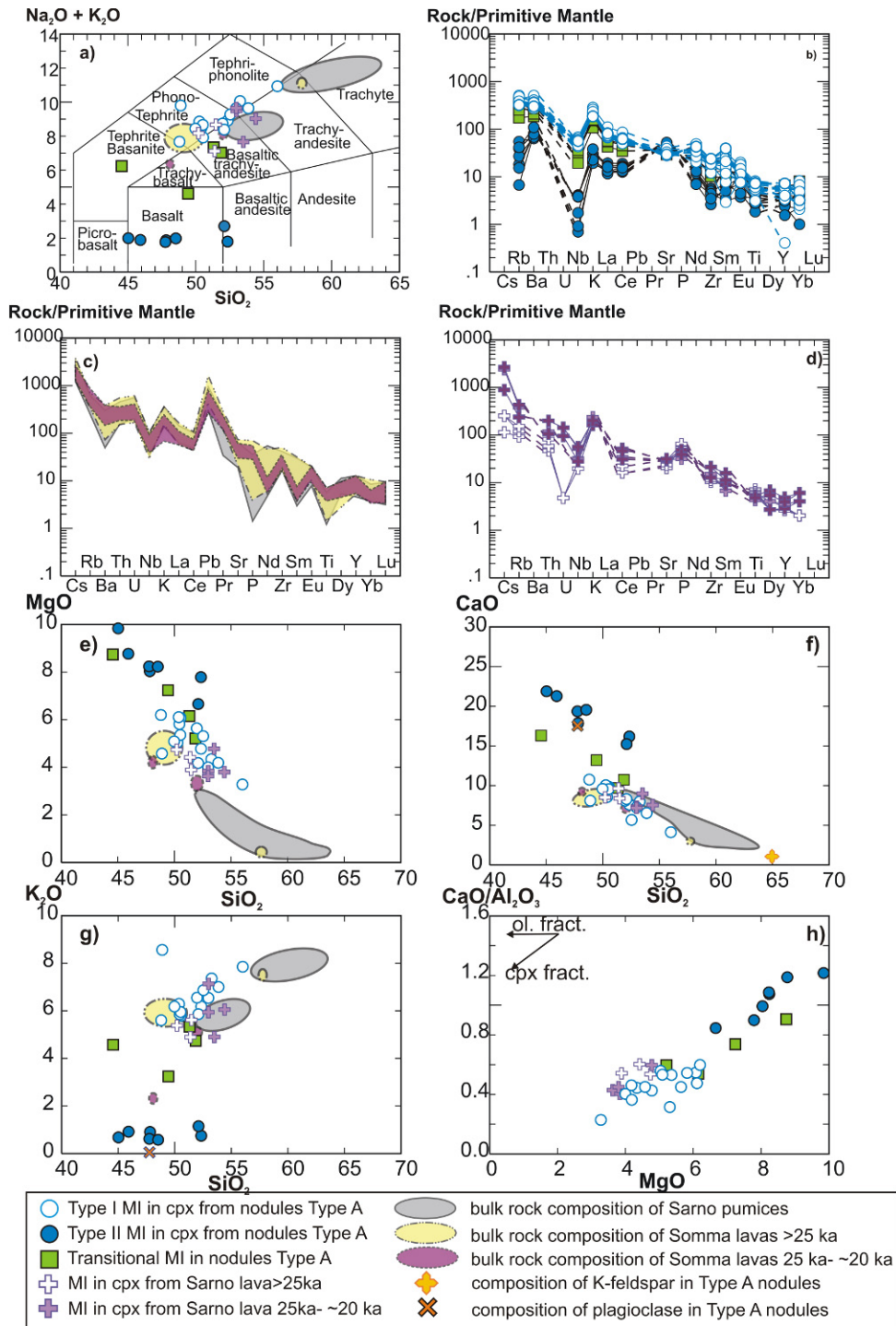


**Figure 5.** Compositions of host rocks, minerals and melt inclusions associated with PB-Sarno nodules. Compositions of crystallized MI were determined by LA-ICP-MS analysis. a) Total alkali – silica diagram [30] showing MI and published bulk rock compositions of associated Somma lavas and pumices, b-d) Primitive mantle-normalized [31] trace element diagram, e)  $\text{SiO}_2$  versus  $\text{MgO}$ , f)  $\text{SiO}_2$  versus  $\text{CaO}$ , g)  $\text{SiO}_2$  versus  $\text{K}_2\text{O}$ , h)  $\text{MgO}$  versus  $\text{CaO}/\text{Al}_2\text{O}_3$ . The arrows on Fig. 3f labeled “cpx fract” and “ol. fract” show the compositional trends in residual melt which would result from clinopyroxene and olivine crystallization, respectively. For comparison, the bulk composition of the pumices erupted during the plinian phase of the PB-Sarno eruption [17, 21], the bulkcompositions of lavas erupted between 35-25 ka [17, 19], of lava and scoria erupted after 25 ka but before the PB-Sarno eruption [19], and compositions of melt inclusions hosted in clinopyroxene from lava erupted between 35 ka and the PB-Sarno eruption [29] are also plotted.

crystal/melt ratio was high. This material was extracted from the crystal mush zone and then transported upwards “slowly and intact, permitting crystallization of the interstitial liquid” [4]. Alternatively, Hermes and Cornell [4] also suggest that the type of nodule described here could represent cumulitic xenocrysts that were extracted from the mush-zones and then mixed with magmas of different compositions within a chemically zoned magma chamber. The rare reverse zoning observed in clinopyroxene and the relatively low-Fo olivine ( $Fo \leq 76$  mol%) inclusions in primitive clinopyroxene ( $mg\# \geq 0.80$ ) indicate that some mixing occurred. However, the lack of typical non-equilibrium textures (e.g. multiple resorption surfaces within a crystal; complex zoning; reaction rims) suggests that the samples more likely represent a crystal mush zone where the crystal/melt ratio was high, rather than mixing with magmas of different composition. The differences between Type A and B nodules suggest that, even though they formed in a similar environment (probably a crystal mush zone at the margins of a magma chamber), they are derived from different regions of a compositionally zoned magmatic system.

The compositions of the crystals in the studied samples are more primitive compared to the crystal aggregates described by Landi et al. [21], which they found in pumices and scorias deposited during the sustained column phase of the eruption (“plinian phase” in [20, 21]). This compositional difference suggests that the nodules in the present study were derived either from a region of the magma chamber that was not sampled during the plinian phase of the eruption, e.g. from the more crystal-rich part that is closer to the margin, or from a different depth in a layered magma chamber. The latter interpretation is consistent with results of Landi et al. [21], who suggest that the magma chamber associated with the PB-Sarno eruption was compositionally layered. As such, the studied nodules were likely entrained as the magma passed through a portion of the magma chamber with a more primitive composition as it ascended to the surface. Various thermobarometers were applied to the mineral assemblages contained in the nodules in an effort to constrain the pressure and temperature of crystallization. The models in Putirka [32] predict temperatures ranging from 1058 to 1264°C and pressures ranging from 3.9 to 10.6 kbar. Additional MI studies, including analysis of MI in Type B nodules as well as analysis of volatiles in MI from both Type A and B nodules, may help to better constrain the PT conditions.

Two very distinctive types of MI were observed in clinopyroxenes from Type A nodules. The two types of MI are spatially associated, which would suggest a genetic relationship, but the nature of this relationship is unclear. The

trace element compositions and the close spatial association of these MI with different compositions indicate that the melts are not differentiated from the same parent melt. Type I MI are in or close to chemical equilibrium with the host and are interpreted to represent the melt from which the surrounding host clinopyroxene crystallized. Type II MI occur in close association with Type I MI, but Type II are not in chemical equilibrium with the host. This suggests that the composition of Type II MI was either modified by accidentally trapped solid phases or that the MI composition reflects heterogeneities within the melt. The high Ca- and low K-contents of Type II MI suggest that trapping and/or dissolution of An-rich plagioclase, which is observed in MI and as solid inclusions in clinopyroxene, might have played a major role in altering the composition of the Type II MI. This process, however, does not explain the high Mg-content of the Type II MI. Mesozoic carbonates with a thickness of  $\sim 8$  km that dip westward from the adjacent Apenninic belt have been detected at a depth of 2–3 km in the Mt. Somma-Vesuvius area [35–37]. Both the high Ca- and Mg contents of Type II MI can be explained by assimilation of dolomite at depth, either by trapping small dolomite crystals in the MI or incorporating dolomite into the parental magma before MI trapping, but stable isotopic data are required to confirm this hypothesis.

Previous studies have reported anomalous MI (e.g. high-Ca inclusions in Fo-rich olivine) occurring together with “normal” MI (i.e. in equilibrium with the host) in the same sample from various mid-ocean ridge and subduction environments [38] (and references therein). Danyushevsky et al. [38] attributed the origin of these anomalous MI to “dissolution-reaction-mixing (DRM) processes”. In a complex magmatic plumbing system consisting of interconnected chambers, each with a well-developed mush zone, the intruding magma batches can react with the much cooler wall-rock and/or material in the semi-solidified crystal-mush zones. In addition to cooling of the intruded magma in the mush zones, phases which are not in equilibrium with the intruded melt may undergo partial dissolution. This may be followed by mixing of the reaction products with the intruded melt to produce hybrid melts that can be trapped as MI. These processes can lead to large localized melt heterogeneities which are then sampled by the crystallizing phases [38]. Danyushevsky et al. [38] emphasize that these anomalous and commonly large inclusions are formed at the edges of the conduit system, where the fresh, hot magma is in contact with the cooler mush-zone. In the center of the magma chamber or conduit, olivine (and other phases) would crystallize in equilibrium with the surrounding melt, and these phenocrysts would not contain anomalous MI.

We suggest a model similar to that of Danyushevsky et al. [38] for the origin of Type II MI in the PB-Sarno nodules. It is well documented that Mt. Somma-Vesuvius has a complex plumbing system consisting of three main levels of magma storage, the two deepest of which represent long-lived reservoirs [39] (and references therein). This geometry provides the opportunity for the formation of extensive mush zones over an extended depth range and P-T conditions [11, 12, 39]. Subsequent interaction of material in these mush zones with the differentiating or upwelling melt and/or the wall rock can occur. The process described by Danyushevsky et al. [38] is consistent with our hypothesis that the Type A nodules represent samples of a crystal-mush zone that was once in contact with the magmas that formed the bulk of the erupted material. However, we are unable to determine the specific location within the overall plumbing system of the mush zone that was sampled, and when in the overall evolution of the system that sampling occurred. The major element composition of the MI overlaps with the composition of the older Somma lavas and their MI, which suggests that the Type A nodules more likely were formed prior to the PB-Sarno plinian eruption. However, because data for the composition of PB-Sarno pumice parental magma is not available, we are unable at this time to test our hypothesis that the nodules formed before the PB-Sarno eruption.

## 8. Conclusions

Petrographic features, including the porphyrogranular texture, slight zonation of the phenocrysts, crystallized melt pockets, and “jagged” edges of crystals, all suggest that nodules collected from the PB-Sarno eruption represent samples of the mush zone of the active plumbing system of Mt. Somma-Vesuvius. Geochemically different but spatially associated MI, and similarities between type A MI and the BP-Sarno bulk rock composition and the composition of older eruptive material, support this hypothesis. The nodules could have crystallized either from the same magma that was erupted during the earlier plinian phase of the PB-Sarno eruption, or from a magma associated with an older eruptive phase. Data obtained from Type I MI may provide valuable information about inferred heterogeneities (layering within the magma chamber) during the early history of the volcano. Further studies are in progress to homogenize the crystallized MI and determine the major and trace element compositions as well as the volatile content of the melts. These data will help to better constrain the structure of the plumbing system and pre-eruptive processes that formed the nodules and led to the BP-Sarno eruption.

## Acknowledgements

The authors would like to thank Rosario Esposito for discussions of melt inclusion systematics, Luca Fedele for help with laser ablation ICP-MS analyses, and Charles Farley for help with Raman analyses. Comments on an earlier version of this manuscript by three anonymous reviewers and by guest editors Miriam Baumgartner and Ron Bakker greatly improved the quality and clarity of the presentation. The research was partially funded by the PhD Programme (XXV Cycle, Coordinated by B. De Vivo) “Internal dynamics of volcanic systems and hydrogeological-environmental risks” of the University of Naples Federico II, (Italy), in collaboration with Virginia Tech in the framework of the Memorandum of Understanding (MoU) signed by the two Universities. This material is based upon work supported in part by the National Science Foundation under Grant no. EAR-1019770 to RJB.

## References

- [1] Tait S.R., Wörner G., Van Den Bogaard P., Schmincke H.-U., Cumulate nodules as evidence for convective fractionation in a phonolite magma chamber. *J. Volcanol. Geotherm. Res.*, 1989, 37, 21–37
- [2] Mattioli M., Upton B.G.J., Renzulli A., Sub-volcanic crystallization at Sete Cidades volcano, Sao Miguel, Azores, inferred from mafic and ultramafic plutonic nodules. *Mineral. Petrol.*, 1997, 60, 1–26
- [3] Holness M.B., Bunbury J.M., Insights into continental rift-related magma chambers: Cognate nodules from the Kula Volcanic Province, Western Turkey. *J. Volcanol. Geotherm. Res.*, 2006, 153, 241–261
- [4] Hermes O.D., Cornell W.C., Petrochemical significance of xenolithic nodules associated with potash-rich lavas of Somma-Vesuvius volcano, NSF final technical report, University of Rhode Island, 1978
- [5] Belkin H.E., De Vivo B., Roedder E., Cortini M., Fluid inclusion geobarometry from ejected Mt. Somma-Vesuvius nodules. *Am. Mineral.*, 1985, 70, 288–303
- [6] Belkin H.E., De Vivo B., Fluid inclusion studies of ejected nodules from plinian eruptions of Mt. Somma-Vesuvius. *J. Volcanol. Geotherm. Res.*, 1993, 58, 89–100
- [7] Gilg H.A., Lima A., Somma R., Belkin H.E., De Vivo B., Ayuso R.A., Isotope geochemistry and fluid inclusion study of skarns from Vesuvius. *Mineral. Petrol.*, 2001, 73, 145–176
- [8] Fulignati P., Kamenetsky V.S., Marianelli P., Sbrana A., Mernagh T.P., Melt inclusion record of immiscibility between silicate, hydrosaline, and carbonate

- melts: Applications to skarn genesis at Mount Vesuvius. *Geology*, 2001, 29, 1043–1046
- [9] Fulignati P., Kamenetsky V.S., Marianelli P., Sbrana A., Fluid inclusion evidence of second immiscibility within magmatic fluids (79 AD eruption of Mt. Vesuvius). *Periodico di Mineralogia*, 2005, 74, 43–54
- [10] De Vivo B., Lima A., Kamenetsky V.S., Danyushevsky L.V., Fluid and melt inclusions in the sub-volcanic environments from volcanic systems: Examples from the Neapolitan area and Pontine Islands, Italy. In: Mineralogical Association of Canada Short Course 36. Montreal, Quebec, 2006, 211–237
- [11] Lima A., Danyushevsky L.V., De Vivo B., Fedele L., A model for the evolution of the Mt. Somma-Vesuvius magmatic system based on fluid and melt inclusion investigations. In: De Vivo B., Bodnar R.J., Melt Inclusions in Volcanic Systems: Methods, Applications, Problems. Developments in Volcanology. Elsevier Press, Amsterdam, 2003, 227–249
- [12] Lima A., De Vivo B., Fedele L., Sintoni F., Milia A., Geochemical variations between the 79 AD and 1944 AD Somma-Vesuvius volcanic products: Constraints on the evolution of the hydrothermal system based on fluid and melt inclusions. *Chem. Geol.*, 2007, 237, 401–417
- [13] De Vivo B., Rolandi G., Gans P.B., Calvert A., Bohrsen W.A., Spera F.J., Belkin H.E., New constraints on the pyroclastic eruptive history of the Campanian volcanic Plain (Italy). *Mineral. Petrol.*, 2001, 73, 47–65
- [14] Brocchini D., Principe C., Castradori D., Laurenzi M.A., Gorla L., Quaternary evolution of the southern sector of the Campanian Plain and early Somma-Vesuvius activity: insights from the Trecase 1 well. *Mineral. Petrol.*, 2001, 73, 67–91
- [15] Santacroce R., Cioni R., Marianelli P., Sbrana A., Sulpizio R., Zanchetta G., Donahue D.J., Joron J.L., Age and whole rock-glass compositions of proximal pyroclastics from the major explosive eruptions of Somma-Vesuvius: A review as a tool for distal tephrostratigraphy. *J. Volcanol. Geotherm. Res.*, 2008, 177, 1–18
- [16] Rolandi G., The eruptive history of Somma-Vesuvius. In: Cortini M., De Vivo B., Volcanism and Archeology in Mediterranean Area. Reserch Signpost. Trivandrum, 1997, 77–88
- [17] Ayuso R.A., De Vivo B., Rolandi G., Seal R.R., Paone A., Geochemical and isotopic (Nd-Pb-Sr-O) variations bearing on the genesis of volcanic rocks from Vesuvius, Italy. *J. Volcanol. Geotherm. Res.*, 1998, 82, 53–78
- [18] De Vivo B., Petrosino P., Lima A., Rolandi G., Belkin H., Research progress in volcanology in the Neapolitan area, southern Italy: a review and some alternative views. *Mineral. Petrol.*, 2010, 99, 1–28
- [19] Paone A., The geochemical evolution of the Mt. Somma-Vesuvius volcano. *Mineral. Petrol.*, 2006, 87, 53–80
- [20] Bertagnini A., Landi P., Rosi M., Vigliargio A., The Pomici di Base plinian eruption of Somma-Vesuvius. *J. Volcanol. Geotherm. Res.*, 1998, 83, 219–239
- [21] Landi P., Bertagnini A., Rosi M., Chemical zoning and crystallization mechanisms in the magma chamber of the Pomici di Base plinian eruption of Somma-Vesuvius (Italy). *Contrib. Mineral. Petrol.*, 1999, 135, 179–197
- [22] Thomas J.B., Bodnar R.J., A technique for mounting and polishing melt inclusions in small (<1 mm) crystals. *Am. Mineral.*, 2002, 87, 1505–1508
- [23] Halter W.E., Pettke T., Heinrich C.A., Rothen-Rutishauser B., Major to trace element analysis of melt inclusions by laser-ablation ICP-MS: methods of quantification. *Chem. Geol.*, 2002, 183, 63–86
- [24] Mutchler S., Fedele L., Bodnar R.J., Analysis Management System (AMS) for reduction of laser ablation ICPMS data. In: Sylvester P., Laser-Ablation-ICPMS in the Earth Sciences: Current Practices and Outstanding Issues. Mineralogical Association of Canada, Vancouver, BC, 2008, 318–327
- [25] Norman M.D., Pearson N.J., Sharma A., Griffin W.L., Quantitative analysis of trace elements in geological materials by laser ablation ICPMS: Instrumental Operating Conditions and Calibration Values of NIST Glasses. *Geostand. Newslett.*, 1996, 20, 247–261
- [26] Roedder E., Origin and significance of magmatic inclusions. *Bull. Mineral.*, 1979, 102, 487–510
- [27] Bodnar R.J., Student J.J., Melt inclusions in plutonic rocks: petrography and microthermometry. In: Webster J.D., Melt inclusions in plutonic rocks. Mineralogical Association of Canada, 2006, 1–25
- [28] Esposito R., Bodnar R.J., Danyushevsky L.V., De Vivo B., Fedele L., Hunter J., Lima A., Shimizu N., Volatile Evolution of magma associated with the Solchiaro eruption in the Phlegrean Volcanic District (Italy). *J. Petrol.*, 2011, 52, 2431–2460
- [29] Belkin H.E., De Vivo B., Török K., Webster J.D., Pre-eruptive volatile content, melt-inclusion chemistry, and microthermometry of interplinian Vesuvius lavas (pre-A.D. 1631). *J. Volcanol. Geotherm. Res.*, 1998, 82, 79–95
- [30] Le Bas M.J., Le Maitre R.W., Streckeisen A., Zanettin B., A chemical classification of volcanic rocks based on the total alkali-silica diagram. *J. Petrol.*, 1986, 27, 745–750
- [31] Sun S.-S., McDonough W.F., Chemical and isotopic

- systematics of oceanic basalts: implications for mantle composition and processes. In: Saunders A.D., Norry M.J., *Magmatism in the Ocean Basins*. - Geological Society Special Publication. 1989, 313-345
- [32] Putirka K., Thermometers and Barometers for Volcanic Systems. In: Putirka K., Tepley III F.J., Minerals, inclusions and volcanic processes. *Mineralogical Society of America*, 2008, 61-120
- [33] Cioni R., Santacroce R., Sbrana A., Pyroclastic deposits as a guide for reconstructing the multi-stage evolution of the Somma-Vesuvius caldera. *Bull. Volcanol.*, 1999, 61, 207-222
- [34] Rolandi G., Bellucci F., Cortini M., A new model for the formation of the Somma Caldera. *Mineral. Petrol.*, 2004, 80, 27-44
- [35] Bruno P.P.G., Cippitelli G., Rapolla A., Seismic study of the Mesozoic carbonate basement around Mt. Somma-Vesuvius, Italy. *J. Volcanol. Geotherm. Res.*, 1998, 84, 311-322
- [36] De Natale G., Troise C., Trigila R., Dolfi D., Chiarabba C., Seismicity and 3-D substructure at Somma-Vesuvius volcano: evidence for magma quenching. *Earth Planet. Sci. Lett.*, 2004, 221, 181-196
- [37] Cella F., Fedi M., Florio G., Grimaldi M., Rapolla A., Shallow structure of the Somma-Vesuvius volcano from 3D inversion of gravity data. *J. Volcanol. Geotherm. Res.*, 2007, 161, 303-217
- [38] Danyushevsky L.V., Leslie R.A.J., Crawford A., Durance P., Melt inclusions in primitive olivine phenocrysts: the role of localized reaction processes in the origin of anomalous compositions. *J. Petrol.*, 2004, 45, 2531-2553
- [39] Piochi M., De Vivo B., Ayuso R.A., The magma feeding system of Somma-Vesuvius (Italy) strato-volcano: new inferences from a review of geochemical and Sr, Nd, Pb and O isotope data. In: De Vivo B., *Volcanism in the Campania Plain: Vesuvius, Campi Flegrei and Ignimbrites*. Elsevier B. V., 2006, Chapter 9: 181-202
- [40] Peccerillo A., *Plio-Quaternary Volcanism in Italy: Petrology, Geochemistry, Geodynamics* Springer, Heidelberg, 2005